Quantum fluctuation effects on hyperfragment formation from Ξ^- absorption at rest on ^{12}C*)

Yuichi HIRATA[a,**)], Yasushi NARA[b], Akira OHNISHI[a], Toru HARADA[c],
and Jørgen RANDRUP[d]

[a] *Division of Physics, Graduate School of Science,*
Hokkaido University, Sapporo 060-0810, Japan
[b] *Advanced Science Research Center, Japan Atomic Energy Research Institute,*
Tokai, Ibaraki, 319-11, Japan
[c] *Department of Social Information, Sapporo Gakuin University, Ebetsu 069-8555,*
Japan
[d] *Nuclear Science Division 70A-3307, Lawrence Berkeley National Laboratory,*
Berkeley, California 94720, USA

(Received September 15, 1998)

Formation mechanisms of single, twin, and double hypernuclei from Ξ^- absorption at rest on ^{12}C are investigated with an refined microscopic transport model, that incorporates the recently developed Quantal Langevin treatment into Antisymmetrized Molecular Dynamics. The quantum fluctuations suppress the formation probability of double hyperfragments to around 10%, which is comparable to the experimental data, and the dynamical formation of twin hyperfragment can be described qualitatively.

§1. Introduction

Among various nuclear fragmentation processes, the hyperfragment formation from the Ξ^- absorption reaction at rest is of primary importance for understanding strangeness in nuclei. First, the Ξ^- absorption is the most effective and the most direct way to produce double Λ nuclei. For example, all three double hypernuclear formation events in which $\Delta B_{\Lambda\Lambda}$ is extracted have been discovered through Ξ^- absorption on light nuclear targets.1) - 3) Double hypernuclei give us valuable information of the low-energy YY interaction, and it might be a doorway to study multi-strangeness systems such as strange baryon matter, which is expected to be realized in neutron stars.4) Because of this importance, further experimental searches for double hypernuclear formation through Ξ^- absorption are being carried out and planned at BNL and KEK.5) - 7) In these experiments, the number of stopped Ξ^- is expected to exceed the existing data by an order of magnitude. Therefore, theoretical studies of the Ξ^- absorption reaction and the resulting fragmentations are urgently needed. Second, in the KEK E176 experiment, one finds interesting frag-

---

*) This work was supported in part by the Grant-in-Aid for Scientific Research (Nos. 07640365, 08239104 and 09640329) from the Ministry of Education, Science and Culture, Japan, and by the Director, Office of Energy Research, Office of High Energy and Nuclear Physics, Nuclear Physics Division of the U.S. Department of Energy under Contract No. DE-AC03-76SF00098.

**) E-mail: hirata@nucl.sci.hokudai.ac.jp , Fax: +81-11-746-5444 mentation patterns, such as ${}^{12}\mathrm{C} + \Xi^- \to {}^{4}_{\Lambda}\mathrm{H} + {}^{9}_{\Lambda}\mathrm{Be}$, in which two single hypernuclei are formed.8), 9) This kind of reaction is called *twin* single hypernuclear formation. It can be regarded as a fission of a $S = -2$ system or an exotic decay, which is unexpected in light nuclei, therefore it may suggest some special characteristics of strangeness in nuclei.

In KEK E176, the estimated number of Ξ^- absorption events at rest on light targets is 31.1 ± 4.8, among which one double hyperfragment formation event and two twin single hyperfragment formation events were observed.10) In addition, they found one event in which $S = -2$ hadronic system is formed (event type (B) in Table I), eight single hyperfragment formation events, and eight other events, in which the visible energy release is greater than 28 MeV (event type (C) in Table I). By using these experimental observations, the lower limits (90% confidence level) of $S = -2$ and $S \leq -1$ sticking probabilities were estimated as 4.8% and 47.6%, respectively.10) In a similar way, we can estimate several lower and upper limits of hyperfragment formation probabilities, as shown in Table II.

Table I. Observed stopped Ξ^- events captured in light nucleus. In events (A), the hyperfragment type (double, twin, or single) is specified. In events (B), a hadronic system with $S = -2$ is formed (double or twin), and at least one hypernuclear weak decay must occur in events (C) ($S = -1$ or -2).

	Hyperfragment	(A)	(B)	(C)
$S = -2$	Double	1	} + 1	} + 8
	Twin	2		
$S = -1$	Single	8		

Table II. Estimated lower and upper limit (90% confidence level) by using the number of events shown in Table I. As for the roughly estimated values, see the text.

Hyperfragment	L. L. (%)			U. L. (%)	Rough Est. (%)
Double	–	} 4.8 10)	} 47.6 10)	77.9	3 – 9
Twin	0.66			81.5	6 – 18
Single	14.5			–	26 – 73
No Hyp. Frag.	–			48.8	–

These upper and lower limits are values which we must respect. However, the statistics is so poor that the constraints on the theory is very loose at present. Therefore, in this paper, we use very crude but plausible estimates of double, twin, and single hyperfragment formation probabilities as follows. One extreme would be to consider that there were no more double and twin hyperfragment formation other than the specified ones. Then the double, twin, and single hyperfragment formation probabilities can be estimated as 3% (=1/31.1), 6% (=2/31.1) and 26% (=8/31.1), respectively. Another extreme is to assume that all the weak decay accompanied by charged particles are observed, and the ratio among the double, twin and single hyperfragment formation is kept. Under this assumption, the probabilities might be estimated as 9% (= 1/11), 18% (=2/11), and 73% (=8/11), respectively. We should note that the probabilities of twin and double hyper fragment formation are comparable.

Various analyses of the Ξ^- absorption reaction have been carried out. These studies range from statistical approaches to direct reaction theories. However, no satisfactory consistent description of double and twin hyperfragment formation is given yet. With statistical decay models of the double hyperon compound nucleus,11) the calculated double hyperfragment formation probability is too large *as* compared with that of twin hyperfragment formation, provided that the $\Lambda\Lambda$ interaction is attractive. Although the relative ratio of double- and twin-hyperfragment is improved if the $\Lambda\Lambda$ interaction is assumed to be repulsive, this assumption contradicts to previously observed double hypernuclei.1) Thus the experimental data suggest the action of some dynamical effects that cannot be mocked up by a simple escape probability of one Λ particle after the primary elementary reaction, $\Xi^- p \to \Lambda\Lambda$. On the other hand, Yamada and Ikeda have proposed an intuitive direct fragmentation picture which is based on the symmetry of the target (^{12}C) wave function:12), 13) When proton s-hole and p-hole states are created in the primary elementary reaction and a highly excited double hypernuclear state is formed, it is fragmented mainly at the doorway stage to various hypernuclei by emitting some nucleons or clusters. Following this picture, they obtain that the excited channels of $^{12}_{\Lambda\Lambda}$Be + p, $^{12}_{\Lambda\Lambda}$B + n, and $^{11}_{\Lambda\Lambda}$Be + d are produced more strongly than other channels, and the calculated $S = -2$ sticking probability is in agreement with the KEK E176 experiment. However, this model still underestimates the twin hypernuclei formation probability.13)

JR

The aim of this paper is to investigate the formation mechanism of single, twin, and double hypernuclei from the Ξ^- absorption at rest on ^{12}C by applying a recently developed microscopic transport model that augments the Antisymmetrized Molecular Dynamics (AMD) model14) by the effect of quantum fluctuations as given by the Quantal Langevin model.15) - 17)

The microscopic transport approach can describe a variety of processes, from fast reactions, such as quasi free processes that are mainly determined by the elementary two-body collisions, to more central reactions where bulk collective motion occurs and the mean-field dynamics is important. In addition, combined with statistical decay models, the light-particle evaporation from moderately excited nuclei can be described. Since we want to extract the contribution of dynamical processes to the hyperfragment formation from the Ξ^- absorption, the applicability to both dynamical and statistical processes is an important advantage of the transport approach.

Among various microscopic transport models, AMD and Fermionic Molecular Dynamics (FMD)18) take account of the fermionic nature of baryons by using antisymmetrized wave packets. This feature makes it possible to describe fragmentation processes due to cluster and nuclear shell effects,14), 18) - 20) which are important for the study of light nuclear system, including hypernuclei.21) Especially two-body collision processes, which are indispensable for the description of nuclear reactions, are incorporated into AMD. Because of these advantages, we adopt AMD combined with statistical decay model as the starting point for studying Ξ^- absorption reactions.

However, even if anti-symmetrized wave packets are employed, the use of product wave functions, whether of Gaussian form or of the Hartree-Fock type, has certain generic shortcomings that may be of specific importance in the present context. In particular, it is usually difficult to describe the dynamical formation of ground-state fragments in the outgoing state. This point was already noted and some remedies were proposed.$^{14),23),24)}$ In the hyperfragment formation problem, for example, Nara et al. suggested the necessity of the direct productions $K^- + \alpha \to \pi^0 + {}^4_\Lambda\mathrm{H}$ in the K^- absorption reaction at rest on clusterized light nuclear targets which cannot be described with only two-body collision terms.$^{24)}$

Another possibly important problem of microscopic transport models concerns the inherent fluctuations associated with wave packets. When the functional space of single-particle wave functions is restricted to Gaussian form and the system is described by a single Slater determinant, the neglected degrees of freedom are expected to cause fluctuations of the retained degrees of freedom. A treatment of this inherent problem has been proposed recently by Ohnishi and Randrup in the form of the Quantal Langevin model.$^{15)-17)}$ With the development of this model, they have discussed the importance of the fact that wave-packet wave functions are not eigenstates of the Hamiltonian operator and thus possess inherent energy fluctuations that affect both the statistical properties and fragmentation reactions in heavy-ion collisions.

The above features may affect the fragmentation from the Ξ^- absorption reaction. First, the observed twin hyperfragments are in their ground states or low excited states. Next, if the excitation energy is shared among all the degrees of freedom, each particle will have a smaller energy than the separation energy and then particle evaporation and fragmentation may be artificially suppressed in molecular dynamics calculations. For example, in the Ξ^- absorption reaction, many large excited fragments like ${}^{13}_{\Lambda\Lambda}\mathrm{B}$ and ${}^{12}_{\Lambda}\mathrm{B}$ are produced in the dynamical simulation of AMD as discussed later. This consideration imposes the importance of the quantum statistical features, which enhances ground-state fragments since internal degrees of freedom of fragments are likely to be *frozen* while the relative motions between fragments are agitated.

Therefore, in this paper, we focus our attention on the effects of the quantum fluctuations. Specifically, we extend the usual AMD transport model to incorporate quantum energy fluctuations in the manner of the Quantal Langevin model. We call the resulting model AMD-QL. We will show that the application of AMD-QL to Ξ^- absorption at rest on ${}^{12}\mathrm{C}$ leads to total formation probabilities of various double hypernuclei of about 10%, when the $\Lambda\Lambda$ interaction is attractive.

This paper is organized as follows: We first briefly describe how we can incorporate quantum fluctuations in wave packet dynamics in the manner of the Quantal Langevin model in Sec. 2. In Sec. 3, we incorporate this quantum fluctuation into AMD, and give the form and the strength of the fluctuation. Then we show our results of hyperfragment formation in Ξ^- absorption at rest in Sec. 4. In Sec. 5, we summarize our work.

§2. Quantum fluctuations in wave packet dynamics

As already mentioned in the introduction, the fluctuations are not fully incorporated in the transport models describing the time evolution of wave packets based on the time-dependent variational principle (TDVP). In a statistical context, this was already pointed out in Refs. 15) - 17), 30). There are some claims that the statistical properties of the wave packet dynamics can be interpreted to be quantal rather than classical by re-scaling the temperature to fit the exact excitation energies and by analyzing the wave function itself through, for example, the single-particle energy spectrum 25), 26). However, this kind of interpretation does not work in the case of fragment formation, since the fragments are described by the centroid parameters of nucleon wave packets. Thus the same authors of Refs. 25), 26) had to introduce additional fluctuations or correlations to describe fragmentation processes. 26) - 29)

Up to now, several origins of fluctuation in wave packet dynamics have been proposed, such as the momentum width in a single-particle wave packet, 27) short-range correlation between nucleons, 28) or the lack of self-consistency between the wave packet and the mean field. 29) In this work, we do not specify the source of fluctuations, but instead require that the quantum statistical equilibrium is approached in the course of the time evolution following the Quantal Langevin model. 15) - 17) This approach has the merit that the equilibrium properties are ensured. On the other hand, since the system approaches the same equilibrium with any fluctuations within the Quantal Langevin model, we have to determine the form and strength of the fluctuation separately to describe dynamics. In this paper, we parametrize the fluctuation in a relatively simple form and seek to determine the allowed range of the fluctuation strength by applying the model to some phenomena with dissipation and/or fluctuation.

In this section, we briefly describe the Quantal Langevin model and its application to dissipative nuclear collective motion, simulated within a simple soluble model, the Lipkin model. 22)

2.1. *Quantal Langevin Model*

The Quantal Langevin model is designed to ensure that the equilibrium properties of the system are in accordance with quantum statistics. In the case of canonical and microcanonical ensembles, the statistical properties are governed by the partition function and the microcanonical phase volume, respectively,

$$\mathcal{Z}(\beta) = \mathrm{Tr}\left(\exp(-\beta\hat{H})\right) = \int d\varGamma\, \mathcal{W}_\beta(\boldsymbol{Z}) \ , \quad \mathcal{W}_\beta(\boldsymbol{Z}) = \langle \boldsymbol{Z}| \exp(-\beta\hat{H}) |\boldsymbol{Z}\rangle \ , \tag{2·1}$$

$$\varOmega(E) = \mathrm{Tr}\left(\delta(E-\hat{H})\right) = \int d\varGamma\, \mathcal{W}_E(\boldsymbol{Z}) \ , \quad \mathcal{W}_E(\boldsymbol{Z}) = \langle \boldsymbol{Z}| \delta(E-\hat{H}) |\boldsymbol{Z}\rangle \ , \tag{2·2}$$

where $|\boldsymbol{Z}\rangle$ represents a parametrized and normalized quantum state, and $\int d\varGamma\, |\boldsymbol{Z}\rangle\langle\boldsymbol{Z}|$ resolves unity. ¿From these expressions, we see that the probability to find a state $|\boldsymbol{Z}\rangle$ is proportional to the statistical weight $\mathcal{W}(\boldsymbol{Z}) = \mathcal{W}_\beta(\boldsymbol{Z})$ or $\mathcal{W}_E(\boldsymbol{Z})$.

To produce the desired equilibrium distribution $\phi(\boldsymbol{Z};t) \propto \mathcal{W}(\boldsymbol{Z}) \equiv \exp(-\mathcal{F}(\boldsymbol{Z}))$, it is possible to adopt the fluctuation-dissipation dynamics described by, for example, the Fokker-Planck equation,

$$\frac{D\phi(\boldsymbol{Z};t)}{Dt} \equiv \frac{\partial\phi}{\partial t} + \{\phi,\mathcal{H}\}_{P.B.} = -\sum_i \frac{\partial}{\partial q_i}\left(V_i - \sum_j M_{ij}\frac{\partial}{\partial q_j}\right)\phi\ , \tag{2·3}$$

$$V_i = -\sum_j M_{ij}\,\frac{\partial\mathcal{F}(\boldsymbol{Z})}{\partial q_j}\ , \tag{2·4}$$

where $\{q_i\}$ are canonical variables satisfying $d\varGamma = \prod_i dq_i$, D/Dt represents the time derivative along the classical path, and $\mathcal{H}$ denotes the classical Hamiltonian. The second relation is recognized as the Einstein relation that follows from the requirement that the equilibrium distribution be a static solution of Eq. (2·3). In numerical simulations, it is easier to treat the corresponding Langevin equation,

$$\frac{Dq_i}{Dt} \equiv \dot{q}_i - \{q_i,\mathcal{H}\}_{P.B.} = V_i + \sum_j g_{ij}\zeta_j\ , \tag{2·5}$$

where the fluctuation matrix $\boldsymbol{g}$ is related to the mobility tensor $\boldsymbol{M}$ through $\boldsymbol{g}\cdot\boldsymbol{g} = \boldsymbol{M}$ and $\zeta(t)$ is the white noise, $\prec \zeta_i^*(t)\,\zeta_j(t')\succ = 2\delta_{ij}\,\delta(t-t')$. Here we have ignored the diffusion-induced drift term.[31] The R.H.S. of Eq. (2·5), which includes both the average drift term and the stochastic diffusion term described with the white noise ζ, is referred to as the *Quantal Langevin* force and it gives the energy fluctuation for the system. This random force arises from the energy dispersion of each wave packet and thus has a purely quantal origin. Numerically Eq. (2·5) can be solved by the finite difference method in which white noise integrated over a short period $\varDelta t$ is treated as a random number following the complex normal distribution generated independently in each time step, multiplied by $\sqrt{2\varDelta t}$.

In a practical application, we use the ansatz for the statistical weight $\mathcal{W}(\boldsymbol{Z})$ by applying the harmonic approximation.[16] For example, the statistical weight in a microcanonical ensemble $\mathcal{W}_E(\boldsymbol{Z})$ is assumed to be a continuous Poisson distribution,

$$\mathcal{W}_E(\boldsymbol{Z}) \propto e^{-\mathcal{H}/D}\,\frac{(\mathcal{H}/D)^{E/D}}{(E/D)!} = e^{-\mathcal{H}/D}\,\frac{(\mathcal{H}/D)^{E/D}}{\varGamma(E/D+1)}\ , \tag{2·6}$$

$$D = \frac{\sigma_E^2}{\mathcal{H}}\ , \quad \sigma_E^2 = \langle\boldsymbol{Z}|\hat{H}^2|\boldsymbol{Z}\rangle - \langle\boldsymbol{Z}|\hat{H}|\boldsymbol{Z}\rangle^2\ , \tag{2·7}$$

where the ground-state energy is subtracted from the energy expectation value $\mathcal{H}$. Here, D denotes a typical energy scale. Since this typical energy scale D depends on $\boldsymbol{Z}$ only weakly in many cases, the drift term is simplified as follows,

$$V_i = -\beta_{\mathcal{H}}\sum_j M_{ij}\,\frac{\partial\mathcal{H}}{\partial q_j}\ , \quad \beta_{\mathcal{H}} = \frac{\mathcal{H}-E}{\sigma_E^2}\ , \tag{2·8}$$

where $\beta_{\mathcal{H}}$ denotes a state dependent inverse temperature modified by quantum correction.[16] With this form of the drift term, the Einstein relation becomes manifest.

In addition, once the energy dispersion σ_E^2 is given, it becomes feasible to solve the Quantal Langevin equation without further complication.

In addition to the appearance of a random force in the equation of motion, we have to take the intrinsic distortion of wave packets into account before making any observation by using the wave packet ensemble. This point can be easily understood by considering the definition of statistical mean value of an observable $\hat{O}$ in canonical ensemble.

$$\prec \hat{O} \succ = \frac{1}{\mathcal{Z}} \mathrm{Tr}\left(\hat{O}\, e^{-\beta\hat{H}}\right) = \frac{1}{\mathcal{Z}} \int d\Gamma\, \mathcal{W}_\beta(\boldsymbol{Z})\, \frac{\langle \boldsymbol{Z}| e^{-\beta\hat{H}/2}\, \hat{O}\, e^{-\beta\hat{H}/2} |\boldsymbol{Z}\rangle}{\langle \boldsymbol{Z}| e^{-\beta\hat{H}} |\boldsymbol{Z}\rangle} \ . \qquad (2{\cdot}9)$$

Since the Boltzmann weight operator $\exp(-\beta\hat{H})$ cannot be treated as a c-number, the distorted wave function $|\boldsymbol{Z}'\rangle = \exp(-\beta\hat{H}/2)|\boldsymbol{Z}\rangle$ is different from the original evolving state, $|\boldsymbol{Z}\rangle$. For example, the distortion operator $\exp(-\beta\hat{H}/2)$ emphasizes the energy eigencomponent with smaller energies and therefore the observed energy $\mathcal{H}_\beta = \langle \boldsymbol{Z}'|\hat{H}|\boldsymbol{Z}'\rangle / \langle \boldsymbol{Z}'|\boldsymbol{Z}'\rangle$ is smaller than $\mathcal{H} = \langle \boldsymbol{Z}|\hat{H}|\boldsymbol{Z}\rangle / \langle \boldsymbol{Z}|\boldsymbol{Z}\rangle$.[16), 17), 32)]

When the total energy E_0 is specified, the wave packets are distributed according to the weight $\mathcal{W}_{E_0}(\boldsymbol{Z})$ in the Quantal Langevin model, as is shown schematically in Fig. 1. Thus the expectation value of the Hamilton operator with the evolving state $|\boldsymbol{Z}\rangle$ can fluctuate around the specified energy. The difference between the evolving state $|\boldsymbol{Z}\rangle$ and the distorted state $|\boldsymbol{Z}'\rangle$ explains why this fluctuation of energy is allowed: When we make any observation, we have to use expectation values with the distorted state $|\boldsymbol{Z}'\rangle = \sqrt{\delta(E_0 - \mathcal{H})}|\boldsymbol{Z}\rangle$, which is an energy eigenstate with the eigenvalue E_0. Therefore, there is no fluctuation in the observed energy, while the fluctuation of the energy expectation value with respect to the evolving state is necessary. We will discuss this point in the next subsection.

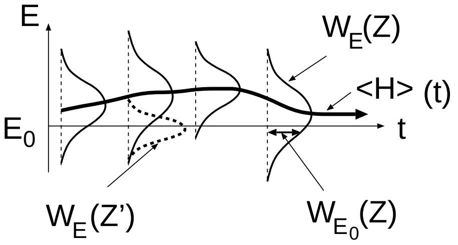

Fig. 1. Fluctuation of the energy expectation value. In the Quantal Langevin treatment with a specified energy E_0, the expectation value with respect to the evolving state $|\boldsymbol{Z}\rangle$ fluctuates (if that wave packet has a component of the eigenstate of the energy E_0). However, any observation involves the distorted state $|\boldsymbol{Z}'\rangle = \exp(-\beta\hat{H}/2)|\boldsymbol{Z}\rangle$.

2.2. *Application to Lipkin Model*

In equilibrium, the Quantal Langevin model has been shown to work very well and give reasonable statistical properties, including the quantum statistical features of simple soluble systems and nuclei.[15) - 17), 30)] In a dynamical context, the fragmentation processes in heavy-ion collisions have been studied.[17)] However, since exact dynamical results are not available, the model has not been verified as a general theory to describe fluctuation-dissipation dynamics. In order to examine this aspect, it may be instructive to employ a schematic model, such as the Lipkin model,[22)] to study the damping of collective motion, since this is one of the most familiar dissipative phenomena in nuclear physics.

The Hamiltonian operator of the Lipkin model,

$$H = \epsilon\, K_0 - \frac{1}{2} V\ (K_+ K_+ + K_- K_-)\ , \tag{2·10}$$

contains only the quasi-spin operators,

$$K_0 \equiv \frac{1}{2}\sum_{n=1}^{N} \left(c^\dagger_{+m}\, c_{+m} - c^\dagger_{-m}\, c_{-m}\right)\ ,\quad K_+ \equiv \sum_{n=1}^{N} c^\dagger_{+m}\, c_{-m}\ ,\quad K_- \equiv (K_+)^\dagger\ . \tag{2·11}$$

Therefore, the collective subspace that couples to the unperturbed ground state $|0\rangle$ completely decouples from other subspaces. Within this collective subspace, the wave packet specified by the complex parameter z,

$$|z\rangle \equiv \exp(zK_+)|0\rangle\ , \tag{2·12}$$

describes a general product wave function which couples to $|0\rangle$. We study the damping of collective motion through the time evolution of this wave packet by using the following Quantal Langevin equation for the canonical variable $w = z\sqrt{N/(1+\bar{z}z)}$,

$$\frac{Dw}{Dt} = \dot{w} - \frac{1}{i\hbar}\frac{\partial\mathcal{H}}{\partial\bar{w}} = -\beta_{\mathcal{H}}\, g^2\, \frac{\partial\mathcal{H}}{\partial\bar{w}} + g\,\zeta\ , \tag{2·13}$$

$$g^2 = \frac{g_0^2\sigma_E}{\hbar}\ ,\quad \sigma_{E}^2 = \frac{\partial\mathcal{H}}{\partial z}\, C^{-1}\, \frac{\partial\mathcal{H}}{\partial\bar{z}}\ ,\quad C = \frac{N}{(1+\bar{z}z)^2}\ . \tag{2·14}$$

When we solve this equation in z space, there naturally appears an N dependence in the coefficient, $g_z^2 \simeq g^2\,\sigma_E/N\hbar$, in the lowest order of z, which comes from the transformation between z and w. We have checked that the qualitative features of the results shown below do not depend on the detailed structure of this coefficient g_z^2, such as its small-z dependence, if this N dependence is preserved.

By using the Langevin Eq. (2·13), we have generated the ensemble of evolving paths. At each time, we have calculated the ensemble average of the operator $\hat{K}_+$ with the distorted wave function, while keeping the evolving state as it is. The strength of the potential is chosen to keep the average potential effect constant. Namely, the following χ parameter is chosen to be independent on N,

$$\chi \equiv \frac{V}{\epsilon}\ (N-1)\ . \tag{2·15}$$

When this parameter is less than unity, the potential energy surface has only one well, while it becomes a double-well shape for $\chi > 1$. As typical examples, we show the calculated results with $\chi = 1.5$ and 0.8 and N=10, 30, and 100, and the initial condition $z(t=0) = 0.6$. As for the fluctuation strength parameter, we show the results with g_0=0.3. However, the qualitative behavior does not change in the wide range of this parameter, $0.1 \leq g_0 \leq 0.5$.

In Fig. 2, we show the time development of $\langle \mathrm{Re}K_+\rangle$, which is related to the collective coordinate. For comparison we also show the exact solution and the results of TDVP by using the above product type wave function. Since the above wave

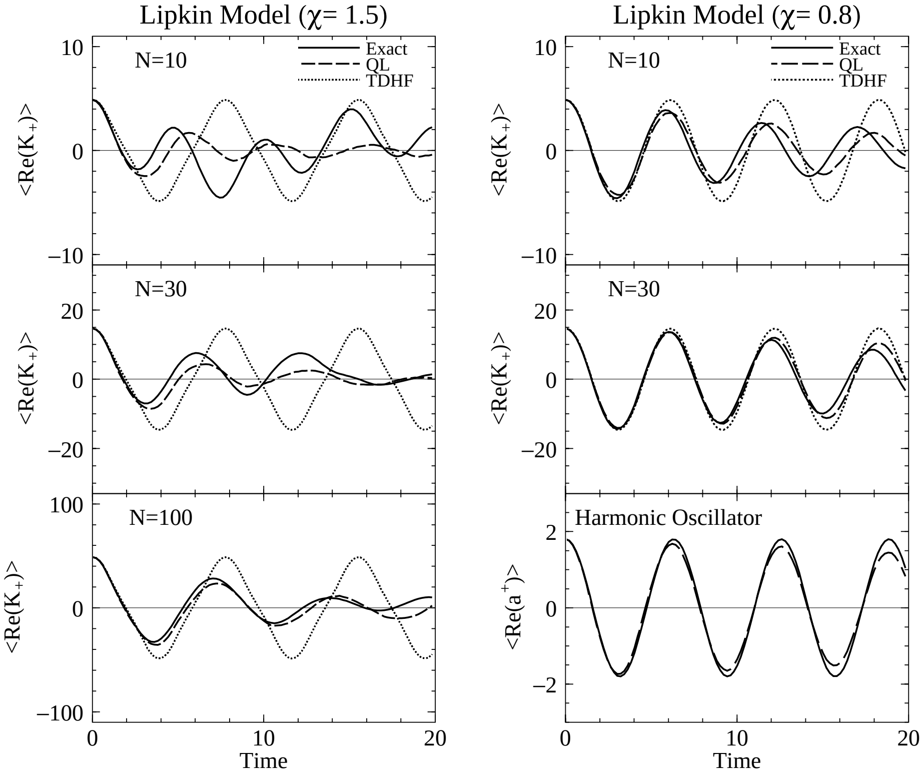

Fig. 2. Damping of collective motion in the Lipkin model. Solid, dotted, and dashed curves show the exact solution and the results of TDHF and the Quantal Langevin model, respectively. The left (right) panels show the results with $\chi = V(N-1)/\epsilon = 1.5$ (0.8), leading to a double (single) potential well. For comparison the bottom-right panel presents the case of the pure harmonic oscillator (one Gaussian wave packet in a harmonic oscillator potential).

function describes a general product wave function, the results of TDVP is nothing but that of the time-dependent Hartree-Fock (TDHF) method. The exact solution shows interesting behavior. At χ=1.5, the collective motion gradually damps at larger N, while for $N = 10$ the collective variable becomes larger again owing to the interference between some specific energy eigencomponents. In addition, we can see some hardening of the collective mode at smaller N. For example, one period becomes much smaller than the TDHF results.

The Quantal Langevin model results exhibit a behavior similar to the exact solution, although it is impossible to treat the interference between some specific energy eigencomponents which agitates the collective motion again after several periods. The average damping width seems to be well reproduced, and more than half of the hardening of this mode is explained. On the other hand, the TDHF result shows a pure periodic motion, since there is only one complex degree of freedom in this wave packet. If the potential strength parameter χ is kept constant, there is no room for N to play any role in TDHF. Therefore, the results of TDHF shows the limit of $N \to \infty$ without any damping.

Within the Quantal Langevin model, the above mentioned damping and hardening can be explained as follows: Each wave packet $|z\rangle$ has its inherent energy fluctuation σ_E which is proportional to $\sqrt{N}$, and in the Quantal Langevin treatment, the energy expectation value of this evolving state can fluctuate around the specified energy with the order of this intrinsic energy fluctuation. Therefore, each wave packet will have different energy expectation value and frequencies and, as a result of ensemble average, the collective motion damps. The hardening of the collective mode is also explained similarly. In the case of χ=1.5 there is a barrier in the potential energy surface at Re(z)=0 and the energy of the initial state is just above this barrier height. In the Quantal Langevin treatment, some of the evolving paths are trapped by this barrier and return to the neighborhood of the initial state much earlier than the classical motion. The first peak of the collective variable for $N = 10$ comes from these evolving states. These features may be related to the strange behavior of collective motion at around the bifurcation point.

When N becomes larger, the importance of the above intrinsic energy fluctuation $\sigma_E \propto \sqrt{N}$ relative to the specified energy $E \propto N$ becomes smaller. Therefore the damping and the hardening of mode become smaller.

In the semi-harmonic case $\chi = 0.8$ the situation is similar. The Quantal Langevin model describes the damping well, but since the potential energy surface is a single well and there is no trapping by the barrier, the behavior of the collective variable is very regular and the damping width becomes smaller. As a limit, we can consider pure harmonic motion. For example, we show in the right-bottom panel of Fig. 2 the time evolution of $\langle a^\dagger \rangle$ in the case of one wave packet in a harmonic oscillator potential. In this case, TDHF (equivalent to AMD in this case) gives the exact solution of the time-dependent Schrödinger equation, while the Quantal Langevin model still gives a small damping. However, this small damping occurs in a special situation and becomes visible only after many periods. Thus it is not a big problem since we are interested in the bulk behavior of dissipative systems such as nuclei.

§3. Antisymmetrized Molecular Dynamics with Quantal Langevin Force

3.1. *Implementation of the Quantal Langevin Force into AMD*

In AMD, the quantum states are constructed by the following Slater determinant of Gaussian wave packets,[14)]

$$|\boldsymbol{Z}\rangle = \frac{1}{\sqrt{A!\ \det \boldsymbol{B}}} \det\Big(|\boldsymbol{z}_i(\boldsymbol{r}_j)\rangle\Big) \ , \tag{3·1}$$

$$|\boldsymbol{z}_i(\boldsymbol{r}_j)\rangle = \left(\frac{2\nu_i}{\pi}\right)^{3/4} \exp\left[-\nu_i(\boldsymbol{r}_j - \boldsymbol{z}_i/\sqrt{\nu_i})^2 + \frac{1}{2}\boldsymbol{z}_i^2\right] \chi_i(j) \ , \tag{3·2}$$

$$B_{ij} = \langle \boldsymbol{z}_i | \boldsymbol{z}_j \rangle \ , \tag{3·3}$$

where χ_i represents the spin-isospin wave function and the parameter ν_i is (inversely) related to the variance of the Gaussian wave packet; both are assumed to remain constant in time. For nucleons we use $\nu_N = 0.16$ fm^{-2}. We have included Λ and Ξ^- particles in the framework of AMD and the width parameters for these particles are chosen to be $\nu_Y = (m_Y/m_N)\nu_N$, where m_Y and m_N are masses of the hyperon and nucleon, respectively. This prescription makes it possible to factorize the center-of-mass wave function. The real and imaginary parts of the parameter $\{\boldsymbol{z}_i\}$ of the Gaussian wave packet (3·2),

$$\boldsymbol{z}_i = \sqrt{\nu_i}\boldsymbol{d}_i + \frac{i}{2\hbar\sqrt{\nu_i}}\boldsymbol{k}_i \ , \tag{3·4}$$

represent the mean position $\boldsymbol{d}_i$ and the mean momentum $\boldsymbol{k}_i$, respectively. Applying the time-dependent variational principle to total wave function $|\boldsymbol{Z}\rangle$,

$$\delta \int dt \ \langle \boldsymbol{Z}| i\hbar \frac{\partial}{\partial t} - \hat{H} |\boldsymbol{Z}\rangle = 0 \ , \tag{3·5}$$

we obtain the equation of motion for the parameters $\{\boldsymbol{z}_i\}$,

$$\frac{D\boldsymbol{z}_i}{Dt} \equiv \dot{\boldsymbol{z}}_i - \frac{i}{\hbar}\boldsymbol{F_i} = 0 \ , \tag{3·6}$$

$$\boldsymbol{F}_i = -\sum_j C^{-1}_{ij} \frac{\partial \mathcal{H}}{\partial \bar{\boldsymbol{z}}_j} \ , \tag{3·7}$$

$$C_{ij} = \frac{\partial^2}{\partial \bar{\boldsymbol{z}}_i \partial \boldsymbol{z}_j} \log \det \boldsymbol{B} \ . \tag{3·8}$$

Here, $\mathcal{H} = \langle \boldsymbol{Z}|\hat{H}|\boldsymbol{Z}\rangle$ is the expectation value of the total energy.

We can construct the Quantal Langevin equation based on the AMD wave functions as before, although there are several points that require special consideration. The first problem is the treatment of the zero-point CM kinetic energies of fragments. 14), 18), 33) Since this fragment zero-point CM kinetic energy is proportional to the number of fragments and does not disappear even in the asymptotic region, it modifies the Q value of fragmentation and suppress fragmentation artificially. This fragment zero-point CM motion also affects the energy dispersion. For example, when one isolated fragment moves the energy fluctuation grows as a linear function of the translational kinetic energy of this fragment. In wave packet dynamics with product-type wave functions, where the fragment CM motion is described by a wave packet, these zero-point kinetic energies are indispensable. However, if we consider a superposition of the wave packets with respect to impact parameter and time in order that the incident wave function be a plane wave as in actual reactions, then the relative phases of this superposition are kept in time and the zero-point CM kinetic energies of the fragments will disappear in the asymptotic region. Therefore, the above effects are spurious and should be removed from the Hamiltonian as well as from the energy dispersion. Several prescriptions for subtracting fragment zero-point CM kinetic energies have already been proposed. 14), 18), 33) As for the calculation of the energy dispersion, we remove these effects by subtracting the local average velocities and forces acting on the wave packets,

$$\sigma_E^2 = \sum_{ij} \bar{\boldsymbol{F}'}_i \cdot C_{ij} \cdot \boldsymbol{F}'_j \ , \tag{3·9}$$

$$\boldsymbol{F}'_i = \boldsymbol{F}_i - \frac{\gamma}{n_i} \sum_k f_{ik} \boldsymbol{F}_k \ , \tag{3·10}$$

where f_{ij} denotes the "friendship" function which is used to subtract the fragment zero-point CM kinetic energies as described later in Subsec. 3.2, n_i is the mass number of the fragment to which the i-th nucleon belongs, and here we use $\gamma = 1$. By this subtraction, the energy fluctuations are correspondingly reduced, thereby ensuring that the fluctuations disappear when all the fragments have become cold.

The second problem concerns the expression of the fluctuation matrix $\boldsymbol{g}$. If we were to adopt a simple constant matrix $\boldsymbol{g}$ having only diagonal terms as in the Lipkin model, both of the translational motion and the intrinsic motion of isolated fragments close to their ground states would be affected by the fluctuation. The first point can be avoided by adopting a fluctuation matrix of the form,

$$g_{ij} \sim \delta_{ij} - 1/A_F \ , \tag{3·11}$$

where A_F is the mass number of the fragment to which the nucleon belongs. On the other hand, the intrinsic (or relative) motion between nucleons are not affected when the same fluctuations are added. Then, we can avoid the second problem by requiring that all the matrix elements of $\boldsymbol{g}$ are similar within an isolated fragment near the ground state. In order to satisfy both requirements approximately, we employ the following matrix $\boldsymbol{g}$ that contains off-diagonal parts reflecting single-particle overlaps,

$$g_{ij} = g_0 \left(\frac{\sigma_E}{\hbar\sqrt{A}}\right)^{1/2} \left(\frac{\tilde{f}_{ij}}{\sqrt{q_i q_j}} - \frac{f_{ij}}{\sqrt{n_i n_j}}\right) \ , \tag{3·12}$$

$$\tilde{f}_{ij} = \exp\left(-\nu_N \left|\frac{\boldsymbol{w}_i}{\sqrt{\nu_i}} - \frac{\boldsymbol{w}_j}{\sqrt{\nu_j}}\right|^2\right) \ , \tag{3·13}$$

where $q_i = \sum_k \tilde{f}_{ik}$. In this form, the diagonal part in Eq. (3·11) is replaced by a narrow Gaussian, and the constant part for each fragment is replaced by a normalized friendship function having a larger width. With this form, the matrix elements of $\boldsymbol{g}$ become almost zero and the energy is unaffected by the fluctuation for fragments close to their ground states. Here we have introduced one free parameter g_0, which governs the overall strength of the fluctuation matrix. We determine this free parameter later in Subsec. 3.4. By using this fluctuation matrix, the Quantal Langevin force is implemented into AMD as follows,

$$\dot{\boldsymbol{z}}_i = \frac{i}{\hbar}\boldsymbol{F}_i + \beta_{\mathcal{H}} \sum_{kl} g_{ik} g_{kl} \boldsymbol{F}'_l + \sum_k g_{ik} \boldsymbol{\zeta}_k \ . \tag{3·14}$$

In addition to introducing a stochastic force in the equation of motion, the Quantal Langevin model requires that the intrinsic distortion of wave packets be taken into account in order to project the state to the appropriate energy shell before making any observation.[16), 17), 32)] In the case where the energy is specified, the distortion operator $\sqrt{\delta(E - \hat{H})}$ is very complicated. Therefore, we have employed the canonical distortion here. This can be done by using the following cooling equation to perform an imaginary-time evolution,

$$\dot{\boldsymbol{z}}_i = \boldsymbol{F}'_i \ , \tag{3·15}$$

until the total energy expectation value reaches the given energy. Although this cooling process hardly influences the fragment configurations at the final stage of the reaction, it reduces the excitation energy of fragments significantly and the energy conservation is completely satisfied after this procedure.

3.2. *Effective Interactions*

We use the following effective interactions in this work. For the NN interaction, the effective interaction Volkov No.1 [34] with Majorana parameter $m = 0.575$ is used. The zero-point kinetic energy ($\mathcal{T}^{CM}$) is subtracted from the Hamiltonian in the same way as in Ref. 14). As a result, the total Hamiltonian is modified to the following form,

$$\mathcal{H} = \langle \boldsymbol{Z}|\hat{H}|\boldsymbol{Z}\rangle - \mathcal{T}^{CM} , \tag{3·16}$$

$$\mathcal{T}^{CM} = T_0 A - a_p T_0 (A - N_F) , \tag{3·17}$$

$$N_F = \sum_i \frac{1}{n_i m_i} , \quad n_i = \sum_j f_{ij} , \quad m_i = \sum_j \frac{f_{ij}}{n_j} , \tag{3·18}$$

$$f_{ij} = \exp\left(-\nu_t \left| \frac{\boldsymbol{z}_i}{\sqrt{\nu_i}} - \frac{\boldsymbol{z}_j}{\sqrt{\nu_j}} \right|^2 \right) . \tag{3·19}$$

Here, $T_0 = 3\hbar^2\nu/2M$ is the zero-point kinetic energy of a fragment, A is the total mass number, and N_F is the number of fragments appearing in the dynamical simulation. The parameters involved in the $\mathcal{T}^{CM}$ are determined as $\nu_t = 0.1$ and $a_p = 0.772$ in order to reproduce the experimental data of binding energies of normal nuclei as shown in Table III.

Table III. Binding energies of single hyper nuclei

Core nucleus		^{3}H	^{4}He	^{7}Li	^{8}Be	^{11}B	^{12}C
B(Core)	cal.(MeV)	10.63	28.30	39.66	56.73	74.51	92.35
	exp.(MeV)	8.48	28.30	39.25	56.50	76.21	92.17
Hypernucleus		$^4_\Lambda$H	$^5_\Lambda$He	$^8_\Lambda$Li	$^9_\Lambda$Be	$^{12}_\Lambda$B	
$B(^A_\Lambda Z)$	cal.(MeV)	12.41	31.43	45.32	60.99	87.15	
	exp.(MeV)	10.52	31.42	46.05	63.27	87.58	
S_Λ	cal.(MeV)	1.78	3.13	5.66	4.26	12.64	
	exp.(MeV)	2.04	3.12	6.80	6.77	11.37	
Fragmentation to				^{3}H+$^5_\Lambda$He	^{4}He+$^5_\Lambda$He		
Q values	cal.(MeV)			3.26	1.26		
	exp.(MeV)			6.15	3.55		

Other interactions ($N\Lambda$, $\Lambda\Lambda$) are assumed to be attractive Gaussian potentials,

$$v_{\Lambda\Lambda} = -90.12 \exp(-0.935 r^2) , \tag{3·20}$$

$$v_{\Lambda N} = -43.62(0.1 - 1.0 P_\sigma + 0.5 P_r) \exp(-0.935 r^2) . \tag{3·21}$$

The range of the $N\Lambda$ interaction is the same as that of two-pion exchange [21] and other parameters are chosen to fit the experimentally known hypernuclear binding energies of $^4_\Lambda$H, $^5_\Lambda$He, $^8_\Lambda$Li, $^9_\Lambda$Be, and $^{12}_\Lambda$B within AMD wave functions as shown in Table III. The largest ambiguity lies in the $\Lambda\Lambda$ interaction, since the information on double hypernuclei is very scarce. We choose the parameter of the $\Lambda\Lambda$ interaction to fit the $\Delta B_{\Lambda\Lambda}$ of ${}^{13}_{\Lambda\Lambda}$B(=4.9 ± 0.7 MeV) obtained in KEK E176 experiment.[3),10)]

In Table III we also show the Λ separation energies and the Q values of some fragmentations that are relevant to this work. These energies are very important, since they largely affect the probabilities of Λ emission and decay to fragments in the dynamical evolution. The adopted effective interactions reproduce the observed separation energies within about 2 MeV, although the separation energies of light clusterized nuclei (${}^{8}_{\Lambda}$Li and ${}^{9}_{\Lambda}$Be) and their Q values of fragmentations (${}^{8}_{\Lambda}\mathrm{Li} \to {}^{3}\mathrm{H} + {}^{5}_{\Lambda}\mathrm{He}$, ${}^{9}_{\Lambda}\mathrm{Be} \to {}^{4}\mathrm{He} + {}^{5}_{\Lambda}\mathrm{He}$) are underestimated a little more because of the limitation of the AMD wave function. We will discuss the consequences of this underestimate later.

3.3. *Two-Body Collisions*

Two-body collisions are also included by using the physical coordinate $\boldsymbol{w}$.[14)] The following elementary collisions are included in our calculations,

$$(1) \quad N + N \to N + N \ , \qquad (3{\cdot}22)$$

$$(2) \quad N + \Lambda \to N + \Lambda \ , \qquad (3{\cdot}23)$$

$$(3) \quad \Lambda + \Lambda \to \Lambda + \Lambda \ , \qquad (3{\cdot}24)$$

where $N = n, p$. The NN cross sections are taken from the experimental data. The cross sections involving Λ are calculated by using the Nijmegen model D.[35)] The Nijmegen model D gives the coupling constants for YN interactions and the cross sections for $N + \Lambda \to N + \Lambda$, assuming a short-range core ($r_c \sim 0.5$ fm) in all the baryon-baryon channels. The cross sections for $\Lambda + \Lambda \to \Lambda + \Lambda$ can be obtained by extending the model D to SU(3) symmetry and keeping the hard-core radius as $r_c = 0.5$ fm.

3.4. *Determination of the fluctuation matrix* $\boldsymbol{g}$ *through proton-induced reactions*

Until now, we have left one free parameter g_0 which gives the overall strength of the Quantal Langevin force. Although this parameter does not affect the statistical properties at equilibrium, it gives the time scale of the relaxation to equilibrium. Thus it has some effect on the dynamics, especially in preequilibrium processes such as fast emission of particles or fragmentation. In this study, we determine the allowed range of the strength parameter g_0 in a phenomenological fashion, by analyzing the fragment production cross sections of the proton-induced reaction on ^{12}C at $E_p =$ 45 MeV, which has a similar excitation energy (43.5 MeV) as that of Ξ^- absorption at rest on ^{12}C (39.5 MeV).

The dynamical simulations are performed with AMD and AMD-QL up to the time 200 fm/c. The decay of the excited fragments produced during the dynamical stage are then treated by the multi-step binary statistical decay model denoted Cascade.[37)] In this manner, we obtain the fragment mass distribution.

First we investigate how normal AMD combined with Cascade works in describing the proton-induced reaction on ^{12}C at 45 MeV. In the upper left panel of Fig 3, we show the results of AMD (histogram) and AMD plus Cascade (open circles) calculation for the fragment mass distribution of ^{12}C+p at 45 MeV. At first glance it

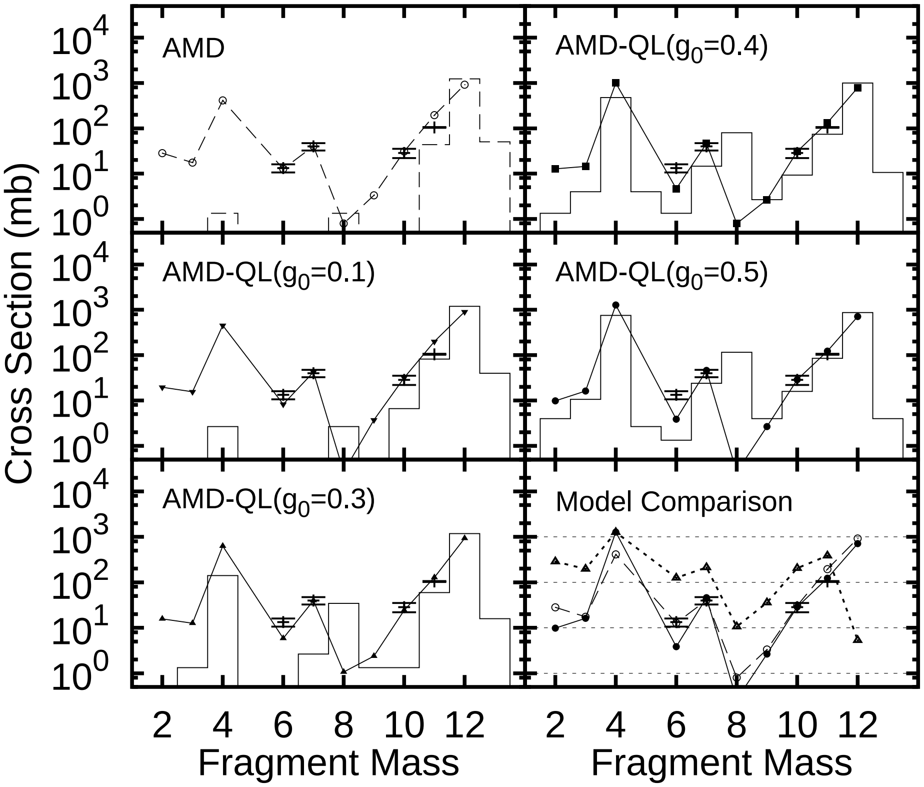

Fig. 3. Calculated fragment mass distribution in the reaction ^{12}C+p at 45 MeV compared with the experimental data. The histograms show the calculated mass distribution at the end of the dynamical stage, while the lines with points show those after the subsequent statistical decay. Dashed and solid lines refer to AMD and AMD-QL, respectively, using $g_0 = 0.1 \sim 0.5$. In the bottom-right panel, we compare the results of AMD and AMD-QL ($g_0 = 0.5$) with the Cascade results starting from pure compound nucleus formation ^{13}N* (dotted line). The maximum impact parameter is taken to be 6.5 fm, which corresponds to a cross section of 1300 mb. The error bars indicate the experimental values.[36)]

seems that the experimental data[36)] is reasonably reproduced. However, in the preequilibrium dynamical stage, which is described by AMD, the fragmentation hardly occurs. One nucleon emission from ^{12}C, inelastic excitation of ^{12}C, and formation of the compound nucleus ^{13}N* are dominant, and most of the intermediate-mass fragments are formed at the statistical decay stage, as already discussed by Takemoto et al.[38)] This description may not be reasonable by the following two reasons. First, the survival probability of the compound nucleus ^{13}N* at the end of dynamical simulation seems too large. The life time of the compound nucleus ^{13}N* at $E^* = 43.5$ MeV is around $\tau \sim 65$ fm/c in Cascade, and the compound-nucleus formation cross section is at most 300 mb, assuming that the grazing impact parameter of around

3 fm. Therefore, at the time t = 200 fm/c when the dynamical calculation ends, around 5% of the compound nuclei ^{13}N* can survive, which corresponds to 15 mb by using the above estimate and well below the calculated value with AMD ($\sim$ 50 mb). The second is the lack of the preequilibrium emissions. Basically Cascade describes low-energy statistical decay of equilibrated excited nuclei and the angular distribution of the ejectiles is isotropic, or at least forward-backward symmetric. However, at these incident energies the fragment angular distribution shows strong forward-backward anisotropy, as shown in the ^{9}Be/^{11}B + p experimental data,[39] caused by direct-like fragment production.

Next we analyze ^{12}C + p at 45 MeV with AMD-QL plus Cascade and seek to determine the allowed range of the parameter g_0 by comparing the calculated fragment mass distribution with data. In Fig. 3, we show the results of the AMD-QL (plus Cascade) calculation for the fragment mass distribution of ^{12}C + p at 45 MeV with g_0=0.1 $\sim$ 0.5. After the statistical decays we cannot see significant differences among the results of the AMD and AMD-QL calculations, and all of them well reproduce the data. However, the mass distribution at the dynamical stage (histograms in Fig. 3) changes drastically when the value of g_0 is changed. As the fluctuation strength is increased from g_0=0 (AMD) to $g_0 = 0.5$, the compound nuclear survival probability decreases and dynamical fragmentation (mainly to α+^{8}Be and 3α) occurs more frequently. We should note that AMD-QL can describe fragmentation to intermediate-mass fragments at low excitation before statistical decay by the effects of fluctuations around classical paths given by Quantal Langevin force. So, the mass distributions before and after Cascade become closer, and direct production of ground-state fragments is partly described with AMD-QL. On the basis of this analysis of proton-induced reactions, we find the range $g_0 \leq 0.5$ for the fluctuation strength parameter is suitable for reproducing the fragment mass distribution after Cascade. In addition, from the consideration of the life-time of compound nuclei and the necessity of preequilibrium fragment emission, the values around $g_0 \sim 0.5$ seems preferable.

It is also possible to describe the reaction ^{12}C + p at 55 MeV with the same value of the strength parameter g_0. Detailed analysis of proton-induced and heavy-ion reactions with AMD-QL will be reported elsewhere.

§4. Results for the Ξ^- absorption reaction

We now apply the AMD-QL simulation, and the subsequent Cascade process, to the absorption of Ξ^- at rest on the nucleus ^{12}C.

4.1. *Initial Condition*

The initial wave function of the Ξ^- hyperon is calculated by assuming the interaction between Ξ^- and ^{12}C to be the following Woods-Saxon potential and the Coulomb potential,

$$U(r) = V_0 \left[1 + \exp(\frac{r-R}{a})\right]^{-1} + U_{Coul}(r) \ , \tag{4·1}$$

where $R = r_0 A^{1/3}$ denotes the nuclear size, and V_0 is the potential depth. Here, we ignore the effects of the imaginary part of V_0 on the wave function. The size and the diffuseness parameters are taken as $r_0 = 1.14$ fm and $a = 0.65$ fm, respectively.

Once the Ξ^- wave function is known, the absorption point of Ξ^- is calculated by the density overlap between Ξ^- and the protons in ^{12}C,

$$\frac{\partial w}{\partial t} \propto \rho_p(\boldsymbol{r})\rho_{\Xi^-}(\boldsymbol{r}) \ . \tag{4·2}$$

It is noteworthy that this density overlap does not depend on the radial quantum number n for higher ℓ if it is normalized, since it is sensitive only to the behavior at the nuclear surface. We assume that Ξ^- always reacts with a proton in ^{12}C and two Λ hyperons are produced at the points where the Ξ^- and proton existed. We neglect the elementary reactions involving the Σ hyperon, since those channles are closed. This elementary reaction is described by ordinary collision term based on the canonical variable $\boldsymbol{w}$.[14] The spins of the produced Λ hyperons are determined statistically. The energy of the Ξ^- absorption on ^{12}C in the experiment in which twin hypernuclei was discovered[8),9)] was well reproduced by a shallow potential ($V_0 = -16$ MeV) and two events of twin hypernuclear formation, $^{12}\mathrm{C} + \Xi^- \to {}^{9}_{\Lambda}\mathrm{Be} + {}^{4}_{\Lambda}\mathrm{H}$, are interpreted as the reactions in which Ξ^- is absorbed from a $2p$ state.[9),40)] In this study, we assume that Ξ^- is absorbed from a (1 or 2)p state and $V_0 = -16$ MeV.

4.2. *Hyperfragment Mass Distribution*

We have made simulation calculations by using AMD and AMD-QL (g_0=0.1, 0.3, 0.4, and 0.5) up to t = 200 fm/c. A few thousand events were generated for each value of the strength parameter g_0. In the case of AMD-QL, we have taken the effects of intrinsic distortion of wave packets into account at the end of the reaction by the imaginary-time evolution given in Eq. (3·15). In this procedure, we have ignored those events in which the total energy expectation value has not reached the specified energy E_0. In the statistical decay stage, the fragment mass and isotope distributions are determined essentially by the Q values of the decay, the Coulomb barrier, and the spin-degeneracy factor. Therefore, we have used the experimentally known hypernuclear binding energies, if available. If not, the separation energies calculated by using the AMD wave functions are adopted. On the other hand, the fragment excitation energies used as the inputs for the statistical decay are calculated by subtracting the calculated ground-state energies in order to avoid the spurious effects arising from the difference between the calculated binding energies in the model space and the experimental values.

In Fig. 4, we show the calculated single and double hyperfragment mass distribution in Ξ^- absorption reaction at rest on ^{12}C with AMD and AMD-QL combined with Cascade.

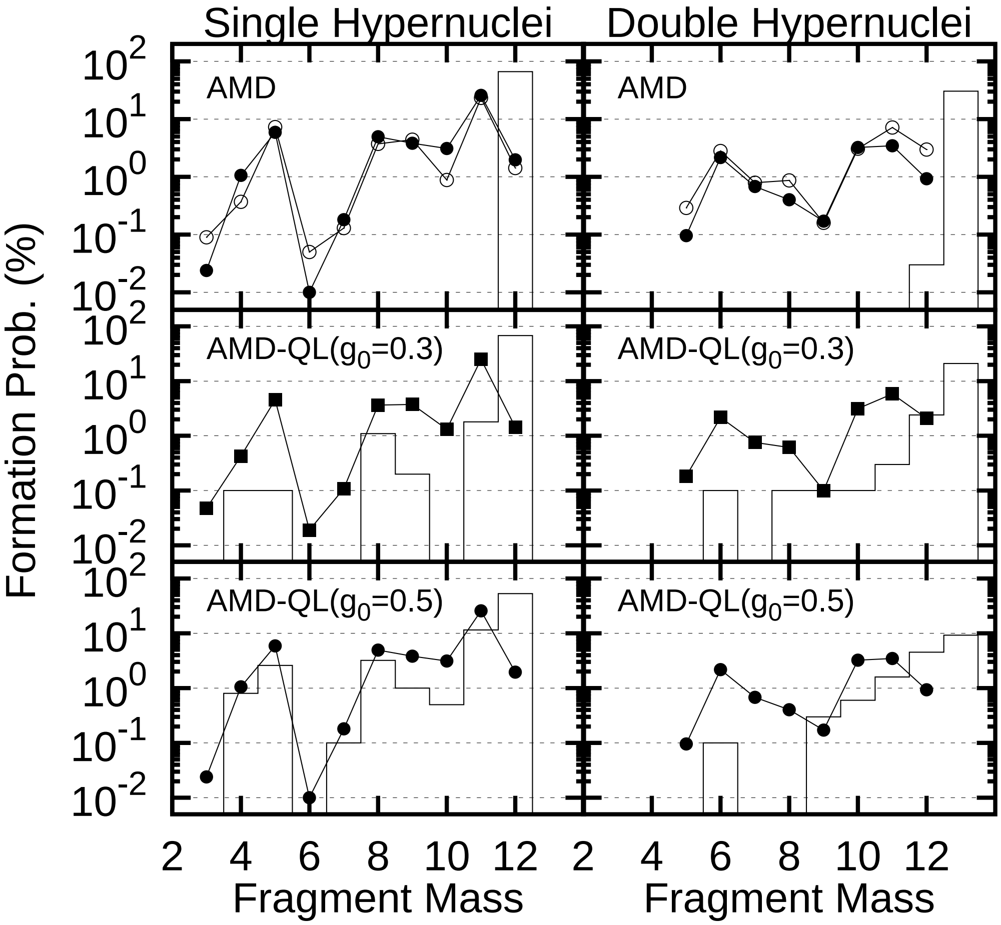

Fig. 4. Calculated single and double hypernuclear mass distributions in Ξ^- absorption reactions at rest on ^{12}C. Histograms in the upper, middle, and lower panels show calculated results with AMD, AMD-QL ($g_0 = 0.3$), and AMD-QL ($g_0 = 0.5$) after the dynamical stage, respectively. Open circles (upper panel), squares (middle), and solid circles (lower) show the results with AMD, AMD-QL ($g_0 = 0.3$), and AMD-QL ($g_0 = 0.5$) followed by Cascade, respectively. For comparison, the upper panel also includes the results for AMD-QL ($g_0 = 0.5$) followed by Cascade.

For the single-hyperfragment mass distribution, the situation is similar to the case of the ^{12}C+p reaction: With AMD, we only obtain formation of the ${}^{12}_{\Lambda}\mathrm{B}^*$ compound nucleus by one Λ evaporation in the dynamical stage. Almost all the single-hyperfragments are formed through the statistical decay of ${}^{12}_{\Lambda}\mathrm{B}^*$ and ${}^{13}_{\Lambda\Lambda}\mathrm{B}^*$. On the other hand, with AMD-QL, fragmentations occur more frequently, mainly to ${}^{11}_{\Lambda}\mathrm{B}$, ${}^{11}_{\Lambda}\mathrm{Be}$, ${}^{8}_{\Lambda}\mathrm{Li}$, and ${}^{5}_{\Lambda}\mathrm{He}$, which have relatively large binding energies and have stable fragmentation partners after one Λ emission. As the fluctuation strength g_0 is increased, dynamical fragmentation enhances. In addition, we can see some signals of the dynamical effect in the single-hyperfragment mass distribution in AMD-QL followed by Cascade. For instance, A=10 (${}^{10}_{\Lambda}\mathrm{Be}$ and ${}^{10}_{\Lambda}\mathrm{B}$) fragments are created mainly through one nucleon (or Λ) evaporation from dynamically produced A=11 single (or double) hyperfragments in AMD-QL followed by Cascade, but these processes are not possible in AMD plus Cascade.

For the double hyperfragment mass distribution, the effects of quantal fluctuations of AMD-QL are more evident. For instance, the production rates of A=11 and 12 double hyperfragments calculated with AMD-QL followed by Cascade are much smaller than those of AMD plus Cascade. This difference comes from the compound nucleus ${}^{13}_{\Lambda\Lambda}\mathrm{B}^*$ formation probability at the end of the dynamical stage. (Although the above difference looks small on a logarithmic scale, it is significant on a linear scale, see Fig. 6.) This formation probability is about 30% in AMD, while it decreases to around 10% for g_0= 0.5 in AMD-QL. In other words, the Λ emission probability is enhanced in AMD-QL.

The *fact* that the formation of long-lived double-hyperon compound nuclei occurs so frequently can be understood as follows. In the initial stage of the Ξ^- absorption reaction, a proton in ^{12}C is converted to a Λ and the residual nucleus becomes ${}^{11}\mathrm{B}^*$. The separation energy of this proton is around 16 MeV, and ${}^{11}\mathrm{B}^*$ is formed with about 6 MeV excitation in AMD. As a result, a large part of the released energy in the elementary reaction of $\Xi^- p \to \Lambda\Lambda$ (28.3 MeV) is expended and the energy available to the 2Λ system is very small ($\sim$ 3 MeV/particle). In AMD, the quantal fluctuations associated with wave packets are neglected and the motion of Λ is limited by the given small energy. Therefore, the formation of long-lived double-hyperon compound nuclei occurs more frequently in AMD calculation.

JR

In order to show the mechanism of Λ evaporation in the dynamical stage of AMD-QL, we analyze the dynamical evolution of the single-particle energy of each of the two produced Λ hyperons. Figure 5 displays a typical time development of two Λ hyperons in a projection showing the single-particle energy and the distance from the center of the nucleus. The left (right) panel is for AMD-QL (AMD) and the initial projections are shown by solid dots. Since in AMD-QL the Quantal Langevin force continually kicks the particles, one of the hyperons is occasionally emitted towards the continuum region, leading to its evaporation from the highly excited ${}^{13}_{\Lambda\Lambda}\mathrm{B}^*$ compound nucleus. In AMD-QL, this type of Λ evaporation process dominates and the double hyperfragment formation is suppressed. By contrast, with the AMD simulation the hyperons are steadily losing their energy, leading to their eventual absorption into the compound nucleus. In this case two hyperons lose most of their single-particle energy as a result of collisions with the nucleons. In AMD this type of energy loss occurs frequently and double-hyperon compound nucleus formation therefore becomes more frequent.

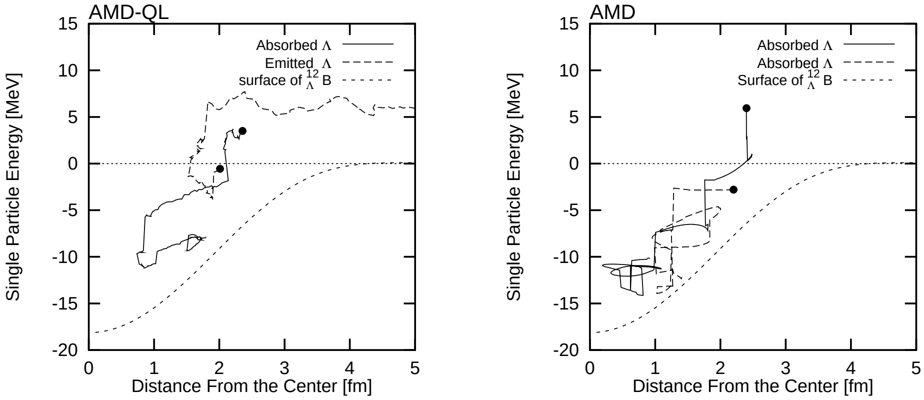

Fig. 5. Typical time development of the single-particle energies of the two Λ hyperons, as obtained with AMD-QL (left) and AMD (right). The abscissa is the distance from the center-of-mass of the system and the ordinate is the single-particle energy. The solid circles indicate the initial position of the hyperons at the time of the $\Xi^- p$ conversion to $\Lambda\Lambda$. The single-particle potential energy of Λ with respect to $^{12}_{\Lambda}$B is shown by the dotted curve. In the AMD-QL simulation, the hyperons are kicked by the random force and one is emitted (dashed trajectory in the left panel). On the other hand, in AMD simulation, even the hyperon that initially had a positive single-particle energy is absorbed into the hyperon compound nucleus due to the energy lost by the collision with a resident nucleon (solid trajectory in the right panel).

It is interesting to compare the ^{12}C + Ξ^- reaction, in which two Λ hyperons are produced, with *the* ^{12}C+p reaction in which all particles are nucleons. In the JR latter case we cannot tell from the mass distribution alone whether the particle was emitted in the dynamical stage or in the statistical stage because the incident (leading) particle and the residents of the target nucleus are identical. Therefore, the mass distribution does not depend on whether the ejectile is the leading particle or arises from the target.

On the other hand, in the Ξ^- absorption reaction, the leading two hyperons are different from nucleons and we can tell whether the ejectile is one of those or not. During the dynamical (or preequilibrium) stage, the probability for leading particle Λ to escape is larger than that for the resident nucleons. However, there is no difference once equilibrium has been achieved. Therefore, we may be able to clarify the contribution of the dynamical fragmentation and statistical one from the Λ emission probability of the Ξ^- absorption reaction.

4.3. *Event Type Analysis*

Table IV shows the dependence on the fluctuation strength parameter g_0 of the relative abundance of different event types; double-, single-, and twin-hyperfragment formation, as well as events with no hyperfragment formation. The AMD results correspond to g_0=0. As described in the previous subsection, quantum fluctuations enhance preequilibrium emission of one Λ particle, while suppressing formation of the double-hyperon compound nucleus $^{13}_{\Lambda\Lambda}\mathrm{B}^*$ (second column in Table IV). This feature also applies to emission of other particles. In the dynamical stage, the double hyperfragment formation probability monotonically decreases and two-Λ emission events (no hyperfragment formation) grows, as g_0 increases. For single hyperfragment formation, it first grows following enhanced one Λ emission, but it saturates and decreases again when two Λ emission becomes visible.

Table IV. Dependence on the fluctuation strength g_0 of the event type abundance (%) for double, single, twin, and no hyperfragment formation. Pure statistical decay results with Cascade and the statistical multifragmentation model [11] are also shown for comparison. In the results of the statistical multifragmentation model, the sum of single and no hyperfragment formation rates is shown with superscript a.

	Dynamical(%)					+Cascade(%)			
g_0	$^{13}_{\Lambda\Lambda}\mathrm{B}^*$	Double	Single	Twin	No Hyp.	Double	Single	Twin	No Hyp.
0.0 (AMD)	30.3	30.3	66.3	0.0	3.4	18.1	39.7	0.9	41.3
0.1	29.6	30.1	66.1	0.0	3.8	18.1	38.4	0.8	42.7
0.3	21.0	24.1	71.3	0.1	4.5	15.1	38.0	0.7	46.1
0.4	16.4	20.4	72.0	0.3	7.3	12.9	42.2	0.9	44.0
0.5	9.2	16.3	70.9	0.9	11.9	11.4	44.0	1.2	43.4
Cascade	100.0	100.0	—	—	—	58.8	24.5	3.1	13.6
Compound [11]	100.0	100.0	—	—	—	66	20^a	14	$—^a$

As the fluctuation strength g_0 is increased, the probabilities after the statistical decay stage generally become closer to those after the dynamical stage. This feature is understood as arising from the quantum statistical nature: In AMD-QL with a sufficient fluctuation strength, a large part of dynamically produced light fragments have excitation energies that are sufficiently small to ensure survival during the statistical decay stage. This is because the lower energy components in the wave packet are emphasized by quantum statistics, as realized in the calculation of the intrinsic distortion of wave packets. Thus the difference between total production rates of hypernuclei at the end of the AMD-QL simulation and after the subsequent statistical decay becomes smaller, while the Cascade after-burner is still important in describing the decay of heavier fragments, such as $^{13}_{\Lambda\Lambda}\mathrm{B}$, $^{12}_{\Lambda\Lambda}\mathrm{B}$, $^{12}_{\Lambda\Lambda}\mathrm{Be}$ and $^{12}_{\Lambda}\mathrm{B}$.

The combined results of AMD and AMD-QL with Cascade show that all of these probabilities are in the allowed range between the lower and upper limits experimentally estimated at 90% confidence level, shown in Table II, and the single hyperfragment formation probability is in the roughly estimated range (26-73%). These things apply at any g_0 value. In addition, with a larger fluctuation strength, the double (twin) hyperfragment formation probability decreases (increases) and becomes closer to the rough estimate 3-9% (6-18%).

In Fig. 6, we show the calculated double- and twin-hypernuclear formation probabilities as a function of the fluctuation strength g_0. At small values of g_0, double hypernuclei are calculated to be formed with a large probability of around 20%. When we incorporate quantum fluctuations, this probability decreases to around 10% at g_0=0.5 due to the enhanced emission of Λ in the dynamical stage. On the other hand, the twin formation probability first becomes smaller at small g_0 values

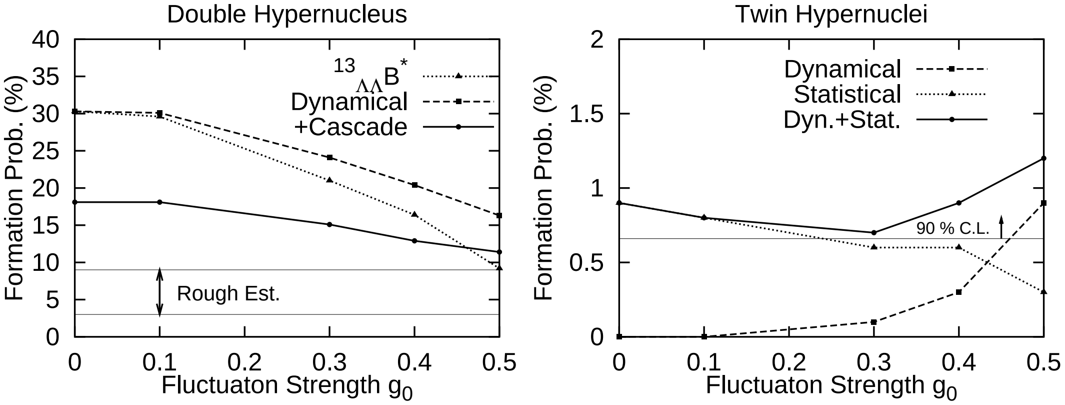

Fig. 6. Double- and twin-hypernuclear formation probabilities as functions of the fluctuation strength parameter g_0. Dashed and solid lines connect the results before and after statistical decays, respectively. The dotted curve in the left panel shows the probability of forming the double-hyperon compound nucleus ($^{13}_{\Lambda\Lambda}\mathrm{B}^*$), and the dotted curve in the right panel denotes the probability of twin hyperfragment formation purely from the statistical decay of the excited double hypernucleus. The experimental estimates are shown by thin solid lines.

and then grows again for $g_0 > 0.3$. Within the model calculation made here, this behavior is governed by the competition between two different formation mechanism of twin hypernuclei; the statistical formation from the double-hyperon compound nucleus and dynamical fragmentation. At small g_0 values, the former dominates twin events and no dynamical formation of twin hypernuclei can be seen. The probability of the latter grows as a linear or quadratic function of g_0, and becomes dominant at large quantum fluctuations, although the twin hyperfragment formation probability is still significantly smaller than the rough estimate.

In Fig. 7 we show the density evolution of a twin hyperfragment ($^{8}_{\Lambda}\mathrm{Li}$+$^{5}_{\Lambda}\mathrm{He}$) formation event obtained with the AMD-QL dynamical simulation. In the initial state, a highly excited $^{13}_{\Lambda\Lambda}\mathrm{B}^*$ compound-like state is formed.

Around 80 fm/c the compound system starts to fission, leading to the formation of the hypernuclei $^{8}_{\Lambda}\mathrm{Li}$ and $^{5}_{\Lambda}\mathrm{He}$ at very small excitation. This twin fragmentation occurs over a relatively long time scale between direct and statistical decay processes. In addition to twin hyperfragments, frequent light-fragment emission (such as $^{4}\mathrm{He}$, $^{3}\mathrm{H}$, and $^{7}\mathrm{Li}$) appear in the dynamical stage of AMD-QL. With quantum fluctuations included we can obtain this variety of

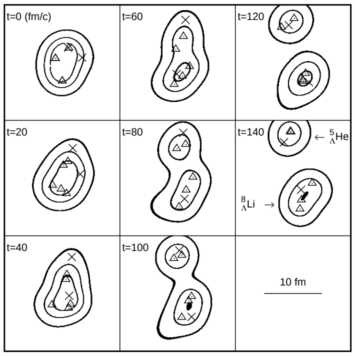

Fig. 7. Time evolution of the matter density in a twin hyperfragment formation event, $^{12}\mathrm{C} + \Xi^- \to {}^{8}_{\Lambda}\mathrm{Li} + {}^{5}_{\Lambda}\mathrm{He}$, calculated with AMD-QL. Crosses and triangles indicate the Λ and proton positions, respectively. Neutrons are omitted for simplicity.

fragmentations during the dynamical stage, before the statistical decay.

4.4. *Exclusive Channels*

Table V shows the calculated rates for various channels with AMD and AMD-QL ($g_0 = 0.5$), both followed by Cascade. We also show the calculated production rates obtained by applying direct reaction theory to the absorption from the $2p$ atomic state of Ξ^- with $V_0 = -16$ MeV.[13] Although they include the production rates to the particle unbound excited states, it is still valuable to compare the trend.

As can be seen in Fig. 4, double hypernuclei are mainly produced at large masses (A=10, 11, and 12), because of their larger 2Λ binding energies. This feature partly explains why it is difficult to detect double hypernuclei, since the non-mesic decay rate is expected to be dominant in these heavier double hypernuclei. One exception is ${}^{6}_{\Lambda\Lambda}$He (lampha), whose production rate reaches around 1.5%. While we can see some visible differences between the results of AMD plus Cascade and AMD-QL plus Cascade, for the reason described in the previous subsection, it is natural that the channels with large Q values are populated abundantly, since a large part of these double hypernuclei are produced through the statistical decay of excited double hypernuclei, ${}^{13}_{\Lambda\Lambda}\mathrm{B}^*$, ${}^{12}_{\Lambda\Lambda}\mathrm{B}^*$, ${}^{12}_{\Lambda\Lambda}\mathrm{Be}^*$.

As for the single hypernuclei, those with mass number A=11 dominate. Once a Λ is emitted, the residual nucleus ${}^{12}_{\Lambda}$B, which has the largest probability in the dynamical stage, will be excited less than 25 MeV, depending on the energy of the emitted Λ. These excitation energies are comparable to the nucleon and Λ separation energies and therefore a single emission is enough to bring the residue into the particle stable regime. The abundant single hypernuclei which are produced from ${}^{12}_{\Lambda}$B, ${}^{11}_{\Lambda}$B, ${}^{11}_{\Lambda}$Be, ${}^{9}_{\Lambda}$Be, ${}^{8}_{\Lambda}$Li, and ${}^{5}_{\Lambda}$He, have their stable decay partners with small separation energies *from* ${}^{12}_{\Lambda}B$, S_n= 12.6 MeV, S_p= 14.1 MeV (AMD calc.), S_t=15.8 MeV, S_α= 13.2 MeV, and $S({}^{5}_{\Lambda}\mathrm{He})$=16.9 MeV, respectively. In AMD-QL, ${}^{10}_{\Lambda}$Be has also a relatively large probability of 1.52%, which is produced through one-nucleon emission from dynamically produced ${}^{11}_{\Lambda}$B and ${}^{11}_{\Lambda}$Be, and deuteron emission from ${}^{12}_{\Lambda}$B. The dominance of heavier single hypernuclei, which mainly decay in non-mesic ways, explains again why we frequently see those events with large energy release without pion (8 events out of an average of 31.1).

In twin hypernuclear formation channels, the difference between AMD and AMD-QL appears most clearly. While all the twin hypernuclear formation is described by the statistical decay of ${}^{13}_{\Lambda\Lambda}\mathrm{B}^*$ in AMD, it is mainly described in the dynamical stage in AMD-QL with a sufficient fluctuation strength. Especially, in the channels ${}^{8}_{\Lambda}$Li+${}^{5}_{\Lambda}$He, $2{}^{5}_{\Lambda}$He+t, and ${}^{5}_{\Lambda}$He+${}^{4}_{\Lambda}$H+α, most of the dynamically produced fragments are bound and therefore survive the statistical decay stage. Another visible channel in the dynamical stage is ${}^{9}_{\Lambda}$Be+${}^{4}_{\Lambda}$H, which is the experimentally observed one. However, in the ${}^{9}_{\Lambda}$Be+${}^{4}_{\Lambda}$H channel, dynamically produced ${}^{9}_{\Lambda}$Be hyperfragments are usually in their particle-unstable states which decay into ${}^{5}_{\Lambda}$He+α. One reason for this instability is the underestimate of the separation energy to the ${}^{5}_{\Lambda}$He+α channel within the present effective interaction and AMD wave function. Another reason might be in the extended density profile of ${}^{9}_{\Lambda}$Be. The fluctuation matrix with the form of Eq. (3·12) is selected so as not to affect the intrinsic motion of well-isolated

Table V. Calculated production rates with AMD and AMD-QL ($g_0 = 0.5$), followed by Cascade, for double, single, and twin hypernuclear formation. The results of direct reaction theory [13] are also shown for comparison. For the value of ${}^{5}_{\Lambda\Lambda}\mathrm{H} + 2\alpha$ in direct reaction theory we take the rate of the ${}^{5}_{\Lambda\Lambda}\mathrm{H}$+^{8}Be channel.

Channel	AMD		AMD-QL($g_0 = 0.5$)		Direct [13]
	Dynamical(%)	+Cascade(%)	Dynamical(%)	+Cascade(%)	
Double Total	30.3	18.07	16.3	11.39	
${}^{13}_{\Lambda\Lambda}$B	30.3	—	9.2	—	
${}^{12}_{\Lambda\Lambda}$B+n	—	2.00	2.4	0.61	3.96
${}^{12}_{\Lambda\Lambda}$Be+p	0.03	0.96	2.1	0.34	2.43
${}^{11}_{\Lambda\Lambda}$B+2n	—	1.57	0.4	1.00	
${}^{11}_{\Lambda\Lambda}$Be+d	—	0.26	0.3	0.09	0.59
${}^{11}_{\Lambda\Lambda}$Be+pn	—	5.27	1.0	2.88	
${}^{10}_{\Lambda\Lambda}$Be+t	—	0.12	0.4	0.03	0.14
${}^{10}_{\Lambda\Lambda}$Be+(dn,pnn)	—	2.91	0.2	3.17	
${}^{9}_{\Lambda\Lambda}$Be+tn	—	—	0.1	0.10	
${}_{\Lambda\Lambda}{}^{9}$Li+$\alpha$	—	0.16	0.2	0.05	0.05
${}^{8}_{\Lambda\Lambda}$Li+αn	—	0.51	—	0.19	
${}^{8}_{\Lambda\Lambda}$He+αp	—	0.36	—	0.24	
${}^{7}_{\Lambda\Lambda}$He +(^{6}Li,αd,αpn)	—	0.79	—	0.49	
${}^{6}_{\Lambda\Lambda}$He+^{7}Li	—	0.23	—	0.13	0.05
${}^{6}_{\Lambda\Lambda}$He+^{6}Li+n	—	0.60	—	0.37	
${}^{6}_{\Lambda\Lambda}$He+α+(t,dn,pnn)	—	1.85	0.1	1.39	
${}^{5}_{\Lambda\Lambda}$H+2α	—	0.29	—	0.09	0.11^{a}
Other	—	0.19		0.23	
Single Total	66.3	39.68	70.9	43.96	
${}^{12}_{\Lambda}$B+Λ	66.3	1.42	53.0	3.24	2.07
${}^{11}_{\Lambda}$B+Λ+n	—	17.79	7.8	20.90	
${}^{11}_{\Lambda}$Be+Λ+p	—	5.39	3.7	5.31	
${}^{10}_{\Lambda}$B+Λ+2n	—	0.01	—	0.01	
${}^{10}_{\Lambda}$Be+Λ+(d,pn)	—	0.79	0.5	1.52	
${}^{9}_{\Lambda}$Be+Λ+t	—	4.20	0.7	2.73	
${}^{9}_{\Lambda}$Be+Λ+dn	—	0.03	—	0.02	
${}^{8}_{\Lambda}$Li+Λ+α	—	3.67	2.9	4.96	
${}^{7}_{\Lambda}$Li+Λ+αn	—	—	0.1	0.10	
${}^{5}_{\Lambda}$He+Λ+^{7}Li	—	6.26	1.1	3.99	
${}^{5}_{\Lambda}$He+Λ+αt	—	0.03	0.7	0.72	
${}^{4}_{\Lambda}$H+Λ+(2α,^{8}Be)	—	0.09	0.4	0.48	
Twin Total	0.0	0.92	0.9	1.22	
${}^{10}_{\Lambda}$Be+${}^{3}_{\Lambda}$H	—	0.08	—	0.01	
${}^{9}_{\Lambda}$Be+${}^{4}_{\Lambda}$H	—	0.16	0.3	0.04	0.22
${}^{9}_{\Lambda}$Be+${}^{3}_{\Lambda}$H+n	—	0.01	—	0.01	
${}^{8}_{\Lambda}$Li+${}^{5}_{\Lambda}$He	—	0.06	0.3	0.33	0.21
${}^{7}_{\Lambda}$Li+${}^{6}_{\Lambda}$He	—	0.05	—	0.01	
${}^{7}_{\Lambda}$Li+${}^{5}_{\Lambda}$He+n	—	0.08	—	0.07	
2${}^{5}_{\Lambda}$He+t	—	0.36	0.2	0.34	
${}^{5}_{\Lambda}$He+${}^{4}_{\Lambda}$H+α	—	0.12	0.1	0.41	

compact fragments. However, ${}^{9}_{\Lambda}$Be has an extended $\alpha\alpha\Lambda$ structure, and so the intrinsic motion will be affected especially when fragments are separating.

The total probability of twin hypernuclear formation shown here is 0.9 – 1.2%, depending on the fluctuation strength. When we limit the initial system to be the double-hyperon compound nucleus ${}^{13}_{\Lambda\Lambda}\mathrm{B}^*$, the Cascade probability resulting in twin hyperfragments is only around $P_{\mathrm{Twin}}({}^{13}_{\Lambda\Lambda}\mathrm{B}^*)$= 3%. On the other hand, this probability amounts to $P_{\mathrm{Twin}}({}^{13}_{\Lambda\Lambda}\mathrm{B}^*)$ =16%, within the hyperon compound nucleus picture,[11] which exceeds the Cascade result by a factor of five. We have found that it is suppressed to be around $P_{\mathrm{Twin}}({}^{13}_{\Lambda\Lambda}\mathrm{B}^*) = 10\%$ and 7% within a statistical multifragmentation model similar to that used in Ref. 11), when we take account of excited levels of daughter fragments with mass number $A \geq 5$ up to either $E^* = E_{\mathrm{thr}} + 2(A-4)$ MeV or infinity, respectively. Therefore, a factor of two may be explained by a different treatment of the excited fragment states at the statistical decay stage. The remaining factor 2-3 may be due to differences in decay scheme.

§5. Summary and Discussion

We have investigated single, twin, and double hypernuclear formation from Ξ^- absorption at rest on ^{12}C by using Antisymmetrized Molecular Dynamics[14] augmented by the Quantal Langevin force[15)-17] (AMD-QL) and followed by the multistep binary statistical decay model (Cascade).[37]

The Quantal Langevin treatment ensures that the dynamical evolution of the system leads towards quantum statistical equilibrium. Such dynamics can be described by the time evolution of a distribution function that satisfies a Fokker-Planck equation, and the equivalent time evolution of the complex wave-packet parameter $\{\boldsymbol{z}_i\}$ is governed by a Langevin-type equation of motion. This model has been shown to work well in a statistical context; it describes the statistical equilibrium properties of simple soluble models and finite nuclei well,[15)-17] and it has been used to study equilibrium properties of argon fluids.[32] Furthermore, it has met with some success in describing the fragment yields in Au+Au collisions at higher energies (100 – 400 MeV/A) where the number of particles are large and the statistical equilibrium may be achieved.[17] Therefore, the model may be expected to work well also in dynamical contexts where pre- or non-equilibrium aspects are important.

In order to show the validity of the Quantal Langevin model in a dynamical context, we first applied it to the damping of collective motion within a simple soluble Lipkin model. It was shown that the damping process is well described within the Quantal Langevin model, including its dependence on the quasi-spin degeneracy N. Although it is difficult to treat the interference between specific energy eigencomponents that agitate the collective motion again after several periods, the early evolution coincides well with that of the exact solution.

On the basis of the above success in the Lipkin model, we then incorporated the Quantal Langevin force into the Antisymmetrized Molecular Dynamics (AMD). In the resulting model, referred to as AMD-QL, the usual AMD equation of motion for $\{\boldsymbol{z}_i\}$ is augmented by the inclusion of the quantum fluctuations, leading to a Langevin-type equation. In order to achieve reliability in the practical applications, we have employed a relatively simple parametrized matrix $\boldsymbol{g}$ and determined the range of the overall fluctuation strength parameter, g_0, by analyzing the fragment mass distribution of ^{12}C+p reaction at 45 MeV, which has an excitation similar to that of the reaction under consideration, Ξ^- absorption at rest on ^{12}C. This analysis shows that although the fragment mass distribution of AMD-QL resembles that of AMD after statistical decays, it is significantly different in the dynamical stage. In AMD, inelastic excitation of ^{12}C, compound nuclear formation, and one-nucleon emission exhaust almost all the events and no fragmentation can be seen. On the other hand, in AMD-QL with a sufficiently large fluctuation strength g_0, various fragmentations occur dynamically and the mass spectrum in the dynamical stage is closer to the final post-Cascade results as g_0 is increased. Considering the lifetime of the compound nucleus ^{13}N* and the predominance of preequilibrium fragmentation (which is evident from the forward-peaked angular distribution of the fragments, as is apparent in the data for the ^{9}Be/^{11}B + p reactions at 45 MeV,[39] for example), it appears that this new framework is superior to AMD, since the incorporation of the quantum fluctuation of the energy leads to a significantly improved description of particle evaporation and fragmentation in dynamical process. AMD-QL can describe the fragmentation of the moderately excited nuclei dynamically. This feature is expected to be especially important for the Ξ^- absorption reaction, because the total excitation energy in this reaction is very small and a large part of stochastic two-body collisions are blocked. The quantum fluctuations should then be the primary source in the system for generating the fluctuations leading towards the various channels in the final state.

We have employed AMD-QL for studying the dynamical mechanisms for Λ emission and twin hyperfragment formation in the Ξ^- absorption reaction. While AMD (plus Cascade) gives large production probabilities for double hypernuclei (18%) and cannot describe twin hyperfragment formation in the dynamical stage, AMD-QL (plus Cascade) suppresses the formation of double hypernuclei (~10%) and achieves a qualitative description of twin hyperfragment formation in the dynamical stage (~0.9% in dynamical stage, and around 1.2% after Cascade). The calculated probabilities of double, single, and twin hyperfragment formation are in the region allowed by the experimental estimate at 90% confidence level shown in Table II. Moreover, the calculated single hyperfragment formation probability is within rough estimate, 26-73%. In addition, the double hyperfragment formation probability becomes very close to the rough estimate, 3-9%, when the fluctuation strength is sufficiently large. This is mainly due to the enhanced Λ emissions. In AMD, even when a Λ has sufficient energy to escape the compound nucleus, it easily loses its energy by two-body collisions before getting out. Therefore, in AMD a Λ can only escape from the nucleus when it is created on the nuclear surface *and* its initial momentum is directed outwards. By contrast, in AMD-QL the quantum fluctuation continually kicks all the particles and a Λ can then be emitted even if it is initially bound. Through these analyses, we conclude that enhanced Λ emission in the preequilibrium stage is essential in describing the bulk dynamics of Ξ^- absorption at rest and the quantum fluctuation given by the form of Eq. (3·12) describes this enhancement well with the overall quantum fluctuation strength parameter g_0 being around 0.5.

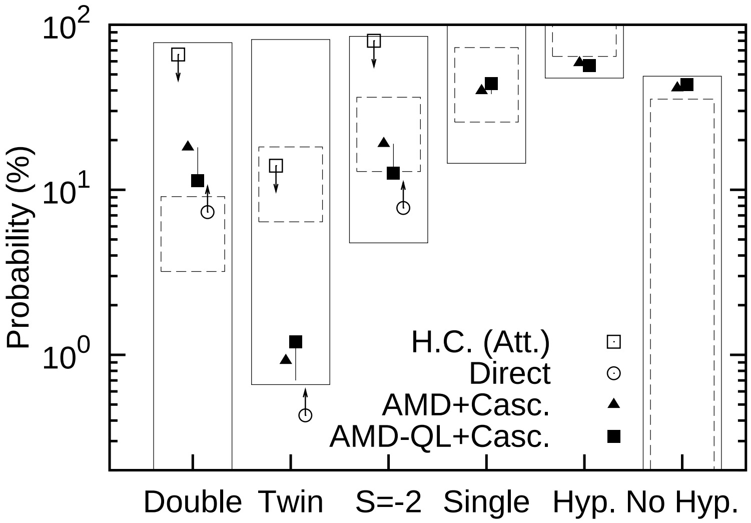

Fig. 8. Various model analyses of relative abundance of the various event types: double, twin, $S = -2$, single, $S \leq -1$, and no hyperfragment formation. Solid triangles and solid squares show the results calculated with AMD and AMD-QL ($g_0 = 0.5$), and the error bars in AMD-QL arise from the fluctuation strength parameter, from g_0 =0 (AMD) to g_0=0.5. The calculated results based on the double-hyperon compound nucleus picture of ${}^{13}_{\Lambda\Lambda}\mathrm{B}^*$ (H.C.) with attractive Λ-Λ interaction[11] and the direct reaction picture for Ξ^- absorption from $2p$ atomic orbit[13] are shown by open squares and open circles, respectively. The arrows from H.C. and direct reaction results show the model uncertainty according to the Λ emission in the preequilibrium stage and multistep processes other than direct break-up, respectively. Experimentally allowed ranges are closed by solid lines (90% confidence level) and dashed lines (rough estimate).

Although the calculated twin hyperfragment formation probabilities are larger than the experimental lower limit (0.66%), it is still much below the rough estimate, 6–18%. Furthermore, both of the two twin hypernuclear formation events are in the channel ${}^{9}_{\Lambda}\mathrm{Be}+{}^{4}_{\Lambda}\mathrm{H}$ and it is known that these twin hypernucleus are formed after Ξ^- is absorbed in ${}^{12}\mathrm{C}$.[8],[9] Therefore the probability for finding the twin hyperfragments ${}^{9}_{\Lambda}\mathrm{Be}+{}^{4}_{\Lambda}\mathrm{H}$ would reach around 13% (=2 events/ (31.1 events (C,N,O) × 0.48 (C))) when the Ξ^- is absorbed in ${}^{12}\mathrm{C}$. The calculated probabilities for this channel are only 0.16% and 0.04%, with AMD and AMD-QL (g_0=0.5), followed by Cascade, respectively. Even if we sum up the probabilities in the channels ${}^{5}_{\Lambda}\mathrm{He}+{}^{4}_{\Lambda}\mathrm{H}+\alpha$ (0.12% and 0.41%) and ${}^{4}_{\Lambda}\mathrm{H}+\Lambda+(2\alpha,{}^{8}\mathrm{Be})$ (0.09% and 0.48%) to compensate the underestimate of the separation energy in ${}^{9}_{\Lambda}\mathrm{Be}$, the total probabilities, 0.37% and 0.93%, are still smaller than the above rough estimate by an order of magnitude.

This underestimate of twin hyperfragment formation is not a specific problem in transport models, and it was already pointed out in previous works. As pointed out by Yamamoto, Sano, and Wakai,[11] the statistical multifragmentation decay model of the double-hyperon compound nucleus also fails to reproduce the experimental fact that the twin hyperfragment formation is more frequent than that of double, assuming that the Λ-Λ interaction is attractive. Yamada and Ikeda[13] also showed that the channels of twin hypernuclei gave very small spectroscopic factors, and the calculated formation probability of twin hypernuclei was very small.

Figure 8, summarizes the results of various model analyses. Since the emission probability of one Λ at the preequilibrium stage is not taken into account in Ref. 11), we assume that the calculated values give the upper limit of the model. On the other hand, the probabilities shown in Ref. 13) for double, twin, and $S=-2$ in the direct reaction picture are considered to be lower limits, since the dissipation of the doorway state into compound states and formation from these compound states are neglected. We can see immediately that all the analyses underestimate the twin hyperfragment formation probability relative to that for double hyperfragment formation.

Therefore, if the twin hypernuclear formation probability, especially in the channel ${}^{9}_{\Lambda}\mathrm{Be}+{}^{4}_{\Lambda}\mathrm{H}$, is really high as suggested, there must be some production mechanism which is missed in all the theoretical works, including this work. Another possibility is that the twin hypernuclear formation probability is very close to or below the lower limit at 90% confidence level estimated by using the number of observed events. In order to distinguish these two possibilities, higher statistics experiments are required. In addition to the higher statistics, one of the key challenges is to narrow down the upper limit in each type of events. This requires resolving the unspecified events, such as those events of type (C) in Table I.

We have noted the shortcomings of the standard microscopic AMD model with which it is hard to describe production of fragments near their ground states in low-energy preequilibrium dynamical processes, such as twin hypernuclear formation. As the inclusion of quantum fluctuations leads to a significant improvement, the extended model may yield a better description of other fission processes as well.

It is obviously important to broaden the confrontation of the theory with experiment through application to other reactions for which suitable data is available. Moreover, it should be kept in mind that there are still ambiguities in AMD-QL. The key quantity concerning fluctuations, the matrix $\boldsymbol{g}$, is determined phenomenologically. Therefore, in the future, it would be of interest to determine $\boldsymbol{g}$ from more fundamental considerations. In this context, we draw attention to a recently developed extended AMD (called AMD-V) that incorporates a diffusion of single-particle wave functions.[29] Since this description also introduces fluctuations of the centroid parameter $\{\boldsymbol{z}_i\}$, it may be helpful in determining the matrix $\boldsymbol{g}$ of the AMD-QL model. Another possibility worth exploring is to incorporate the effects of two-particle correlations and their propagation[41] in a statistical manner. We hope that these challenges will help to deepen our microscopic understanding of fluctuation and dissipation phenomena in nuclear dynamics.

Acknowledgements

The authors thank Prof. S. Shinmura, Prof. K. Katō, Prof. K. Imai, Dr. I. Fuse, Prof. M. Oka, Prof. K. Matsuyanagi, Prof. K. Nakazawa, and Dr. A. Ono for valuable discussions and suggestions, and all the members of the Nuclear Theory Group in Hokkaido University for their great encouragements. This work was supported in part by the Grant-in-Aid for Scientific Research (Nos. 07640365, 08239104 and 09640329) from the Ministry of Education, Science and Culture, Japan, and by the Director, Office of Energy Research, Office of High Energy and Nuclear Physics, Nuclear Physics Division of the U.S. Department of Energy under Contract No. DE-AC03-76SF00098.

References

1) M. Danyz *et al.*, Nucl. Phys. **49** (1963), 121.
2) D. J. Prowse, Phys. Rev. Lett. **17** (1966), 782.
3) S. Aoki *et al.*, Prog. Theor. Phys. **85** (1991), 1287.
4) N. Itoh, Prog. Theor. Phys. **44** (1970), 291;
N. K. Glendenning, Phys. Lett. **B114** (1982), 392;
G. E. Brown, C. Lee, M. Rho, and V. Thorsson, Nucl. Phys. **A567** (1994), 937;
J. Schaffner and I. N. Mishustin, Phys. Rev. **C53** (1996), 1416.
5) M. May and G. B. Franklin, AGS proposal E885.
6) T. Fukuda and R. E. Chrien, AGS proposal E906 (1994).
7) K. Nakazawa, Nucl. Phys. **A585** (1995), 75c.
8) S. Aoki *et al.*, Prog. Theor. Phys. **89** (1993), 493.
9) S. Aoki *et al.*, Phys. Lett. **B355** (1995), 45.
10) K. Nakazawa, in *Proc. of the 23rd INS International Symposium on Nuclear and Particle Physics with Meson Beams in the 1 GeV/c Region, Tokyo, Japan, Mar. 15-18, 1995*, edited by S. Sugimoto and O. Hashimoto (Universal Academy Press, Inc., Tokyo, Japan, 1995), p. 261.
11) Y. Yamamoto, M. Sano, and M. Wakai, Prog. Theor. Phys. Suppl. **117** (1994), 265.
12) T. Yamada and K. Ikeda, Prog. Theor. Phys. Suppl **117** (1994), 445.
13) T. Yamada and K. Ikeda, Phys. Rev. **C56** (1997), 3216.
14) A. Ono, H. Horiuchi, T. Maruyama, and A. Ohnishi, Prog. Theor. Phys. **87** (1992), 1185; Phys. Rev. Lett. **68** (1992), 2898; Phys. Rev. **C47** (1993), 2652; A. Ono, H. Horiuchi, and T. Maruyama, Phys. Rev. **C48** (1993), 2946.
15) A. Ohnishi and J. Randrup, Phys. Rev. Lett. **75** (1995), 596.
16) A. Ohnishi and J. Randrup, Ann. Phys. **253** (1997), 279.
17) A. Ohnishi and J. Randrup, Phys. Lett. **B394** (1997), 260.
18) H. Feldmeier, Nucl. Phys. **A515** (1990), 147;
H. Feldmeier, K. Bieler, and J. Schnack, Nucl. Phys. **A586** (1995), 493.
19) Y. Kanada-En'yo, H. Horiuchi, and A. Ono, Phys. Rev. **C52** (1995), 628.
20) N. Itagaki, A. Ohnishi, and K. Katō, Prog. Theor. Phys. **94** (1995), 1019.
21) T. Motoba, H. Bandō, K. Ikeda, and T. Yamada, Prog. Theor. Phys. Suppl. **81** (1985), Chap. 3.
22) H. J. Lipkin, N. Mechkov, and A. J. Glick, Nucl. Phys. **62** (1965), 188; 199; 211.
23) P. Danielewicz and G. F. Bertsch, Nucl. Phys. **A533** (1991), 712.
24) Y. Nara, A. Ohnishi, and T. Harada, Phys. Lett. **B346** (1995), 217.
25) J. Schnack, H. Feldmeier, Nucl. Phys. **A601** (1996), 181.
26) A. Ono and H. Horiuchi, Phys. Rev. **C53** (1996), 2341.
27) A. Ono and H. Horiuchi, Phys. Rev. **C53** (1996), 845.
28) J. Schnack and H. Feldmeier, Phys. Lett. **B409** (1997), 6.
29) A. Ono and H. Horiuchi, Phys. Rev. **C53** (1996), 2958.
30) A. Ohnishi and J. Randrup, Nucl. Phys. **A565** (1993), 474.
31) H. Risken, *The Fokker-Planck Equation* (Springer, New York, 1989).
32) A. Ohnishi and J. Randrup, Phys. Rev. **A55** (1997), 3315R.
33) D. Kiderlen and P. Danielewicz, Nucl. Phys. **A620** (1997), 346.
34) A. Volkov, Nucl. Phys. **74** (1965), 33.
35) M. M. Nagels, T. A. Rijken, and J. J. de Swart, Phys. Rev. **D15** (1977), 2547.
36) C. T. Roche, R. G. Clark, G. J. Mathews, and V. E. Viola, Jr., Phys. Rev. **C14** (1976),

410.
37) F. Pühlhofer, Nucl. Phys. **A280** (1977), 267.
38) H. Takemoto, H. Horiuchi, and A. Ono, Phys. Rev. **C57** (1998), 811.
39) R. M. Devries, J. W. Sunier, J.-L. Perrenoud, M. Singh, G. Paic, and I. Slaus, Nucl. Phys. **A178** (1972), 417.
40) S. Tadokoro, H. Kobayashi, and Y. Akaishi, Nucl. Phys. **A585** (1995), 225c.
41) M. Gong and M. Tohyama, Z. Phys. **A335** (1990), 153;
M. Gong, M. Tohyama, and J. Randrup, Z. Phys. **A335** (1990), 331.